



ORIGINAL RESEARCH ARTICLE

# Effect of Growth Temperature on Morphological, Structural, and Optical Properties of ZnO Nanorods Using Modified Chemical Bath Deposition Method

AHMED FATTAH ABDULRAHMAN,<sup>1</sup> SABAH MOHAMMED AHMED,<sup>2</sup>  
SAMIR MUSTAFA HAMAD,<sup>3</sup> and AZEEZ ABDULLAH BARZINJY<sup>4,5,6</sup>

1.—Department of Physics, Faculty of Science, University of Zakho, Kurdistan Region, Iraq.  
2.—Department of Physics, College of Science, University of Duhok, Kurdistan Region, Iraq.  
3.—Scientific Research Centre, Soran University, Soran-Erbil, Kurdistan Region, Iraq.  
4.—Department of Physics, College of Education, Salahaddin University-Erbil, Erbil, Iraq.  
5.—Physics Education Department, Faculty of Education, Tishk International University, Erbil, Iraq. 6.—e-mail: azeez.azeez@su.edu.krd

Zinc oxide (ZnO) nanorods (NRs) have been investigated as a function of different growth temperature using modified chemical bath deposition (M-CBD) method. In this study, air bubbles were utilized inside the growth solution as an original modified process. The synthesis of ZnO NRs was carried out through two steps. The first step was deposition of the ZnO seed layer on the glass substrate, while the second step was growing the ZnO NRs on the seeded substrate. The impacts of the growth temperature on the morphology and crystal structure of the ZnO samples were investigated using field emission scanning electron microscopy and x-ray diffraction. UV-Vis spectroscopy was also utilized to characterize the optical properties of the ZnO NRs. The results showed that the growth of the ZnO samples is a NRs-like shape. The ZnO samples possess the hexagonal wurtzite structure with high crystal quality, and no other phases from the impurity were observed. Additionally, the ZnO NRs were found to be well oriented along the (002) planes with diameters ranging from 71 nm to 328 nm and length from 294 nm to 2475 nm, while the aspect ratio was up to 25 with different growth temperatures. However, the UV-Vis spectrum showed that the optical transmittance of the ZnO NRs dropped from ~ 66% to ~ 3.3%, and the absorption band edge had been shifted to a lower-energy region as the growth temperature increased from 65°C to 95°C. This is possibly due to the scattering increase and absorption light from voids, grain size, and thickness of the ZnO NRs. Therefore, it has been demonstrated that the ZnO NRs grown by the M-CBD method at a growth temperature of 95°C gives the most favorable result, since the NRs possess the optimum, homogenous, and uniform distribution with a higher aspect ratio, crystal quality, crystal size, and band gap energy.

**Key words:** ZnO nanorods, growth temperature, modified CBD, optical properties, seed layer

## INTRODUCTION

Zinc oxide (ZnO) is a group-II oxide compound semiconductor with a hexagonal wurtzite structure, and it has a direct band gap energy of 3.3 eV which makes it useful for built-up short wavelength

optoelectronic applications.<sup>1</sup> ZnO is transparent to visible light and can be highly conductive by doping. However, ZnO is one of the most promising materials, due to its well-defined optical and electrical properties, chemical stability, non-toxicity, and even being resilient to radiation damage, which makes it suitable for space applications, as well as the strength and flexibility for wet chemical etching, and thus providing an opportunity for the fabrication of small-sized devices.<sup>2</sup> Moreover, ZnO is recognized as an ecological and economical material.<sup>3</sup> Due to the above-mentioned characteristics, it has shown a remarkable potential in numerous applications, including transparent electrodes in solar cells,<sup>4</sup> UV and blue light emitters,<sup>5</sup> thin film transistors,<sup>6</sup> piezoelectric devices,<sup>7</sup> and gas sensors.<sup>8</sup>

Different topographies of ZnO nanostructures have been fabricated, including nanorods (NRs), nanowires (NWs), nanorings, nanoparticles, quantum dots, nanocombs, nanosheets, nanobelts, nanotubes, and others that have been obtained previously.<sup>9</sup> The above-mentioned ZnO nanostructures can be synthesized using different growth methods, including chemical bath deposition (CBD) method, pulsed laser deposition, molecular beam epitaxy, RF sputtering, chemical vapor deposition, electrochemical deposition, spray pyrolysis, sol-gel method, hydrothermal method, and a modified chemical bath deposition method.<sup>10</sup> Among these methods, due to its many advantages, the CBD approach is attracting great attention from researchers.<sup>11</sup> Also, CBD possesses high-performance, most effective, and efficient fabrication methods for growing several nanostructures. CBD can be conducted at low temperatures ( $> 100^{\circ}\text{C}$ ). Moreover, it is inexpensive, simple, reproducible, non-hazardous, high-density array forming using environmentally friendly chemicals, starting chemicals are commonly cheap and available, and deposition is possible on a large range of substrates.<sup>12</sup> Nevertheless, there are some disadvantages and limitations associated with the CBD method which have been reported in the literature.<sup>13</sup> However, these disadvantages and limitations have been modified and addressed using an inexpensive modified CBD method.<sup>14</sup> The modification has been carried out using injections of air bubbles inside the growth solution during the CBD reaction in an oven to provide a continuously homogenous growth solution and to furnish the oxygen for the duration of the CBD process.<sup>15</sup> The surface morphology, size, shape, and alignment of ZnO NRs grown using the modified CBD method can be controlled by adjusting the different main growth conditions and preparation parameters, such as the growth (bath) temperature, the reaction time, the precursor concentration of reactants in the growth solution, the pH value of the reactant solution, and the seed layer thickness.<sup>14</sup> However, the growth temperature is the leading growth parameter, which has a significant and critical effect on the production of ZnO

nanostructures.<sup>16</sup> It can be stated that the growth temperature is the crucial parameter in order to find the chemical and physical properties of ZnO NRs array.<sup>11</sup> Also, the morphology, length, size, aspect ratio, and growth rate have a direct influence by adjusting the growth temperature.<sup>17</sup>

In fact, many researchers have investigated the effect of different growth (bath) temperatures on the characteristic properties of ZnO NRs. For instance, Kamruzzaman and Zapien<sup>18</sup> studied the effect of the growth temperature ( $80\text{--}90^{\circ}\text{C}$ ) on the morphology of synthesized ZnO NRs. Holi et al.<sup>19</sup> investigated the significant effect of the growth temperatures ( $75^{\circ}\text{C}$ ,  $85^{\circ}\text{C}$ , and  $95^{\circ}\text{C}$ ) on grown ZnO NRs. Nandi et al.,<sup>20</sup> reported that it is possible to control the aspect ratio of ZnO NRs on the substrate by changing the preparation growth temperature. Gawali et al.<sup>21</sup> reported that variation in the growth temperature may change the pH values of the growth solution and morphology conversion of ZnO NRs to nanotubes. Safa et al.,<sup>22</sup> reported that the growth temperature ( $50\text{--}110^{\circ}\text{C}$ ) had an effect on the aspect ratio of ZnO NRs. Farhat et al.<sup>23</sup> stated that the growth temperature has a great influence on the growth, orientation, and aspect ratio of ZnO NRs. Abdulrahman et al.<sup>24</sup> proposed the role of growth temperatures on well-aligned, morphology, optical properties, and energy band gap of ZnO NRs on Si substrates by using the CBD method at low temperature. They also reported that the controllable growth of ZnO NRs can be realized by changing the preparation conditions. Zhang et al.<sup>25</sup> prepared ZnO NRs grown on ITO substrates by the CBD method. In their study, the influence of different growth temperatures ( $70^{\circ}\text{C}$ ,  $80^{\circ}\text{C}$ , and  $90^{\circ}\text{C}$ ) on the crystal structure, surface morphology, and optical properties of ZnO NRs were covered. They also reported that the size of the nano-crystals is increased and their average diameter decreased as the growth temperatures are increased.<sup>25</sup> In another investigation, the effect of different growth temperatures ( $70^{\circ}\text{C}$ ,  $80^{\circ}\text{C}$ ,  $90^{\circ}\text{C}$ , and  $100^{\circ}\text{C}$ ) on the performance of ZnO NRs on ITO substrate-based thin film solar cells by a chemical solution method were observed by Ghosh et al.<sup>26</sup> who reported that the growth temperature plays an important role in the production of different ZnO nanostructures. A high solar cell efficiency was found when ZnO NRs grew at  $80^{\circ}\text{C}$ .<sup>27</sup> Duoc et al.<sup>28</sup> synthesized ZnO NRs at different growth temperatures ( $60\text{--}90^{\circ}\text{C}$ ) grown on a flexible Phynox alloy substrate by using a low-temperature solution method for 4 h. It was found that the diameter, length, and aspect ratio of the ZnO NRs were changed with the change of growth temperature. Goel et al.<sup>29</sup> researched the influence of different growth temperatures ( $70\text{--}100^{\circ}\text{C}$ ) on ZnO NRs properties and the performance of dye-sensitized solar cells, showing that the heights, diameter, surface densities, and regularity of the ZnO NRs were increased as the growth temperatures increased.

In this study, ZnO NRs have been synthesized by using a modified CBD method in a temperature range from 65°C to 115°C. The impact of different growth temperatures on the surface morphology, top view, cross-section (growth direction and length), elemental chemical composition, structure, and optical properties of the ZnO NRs have been systematically investigated.

## EXPERIMENTAL DETAILS

In this study, all the chemicals materials used, such as zinc nitrate hexahydrate (ZNH) ( $\text{Zn}(\text{NO}_3)_2 \cdot 6\text{H}_2\text{O}$ ) and hexamethylenetetramine (HMTA) ( $\text{C}_6\text{H}_{12}\text{N}_4$ ) were purchased from Sigma-Aldrich without further purification. Deionized water with a resistivity of 18.2 M $\Omega$  cm has been used in the fabrication and treatment processes.

### ZnO Seed Layer Preparations

Microscope glass substrates have been selected for growing the ZnO NRs. The glass substrates were cleaned in an ultrasonic bath by using ethanol, acetone, and deionized water for 25 min each and then dried with nitrogen gas. Radio frequency (RF) magnetron sputtering was employed using a ZnO target (99.99% purity of ZnO) to deposit a 80-nm ZnO seed layer on the substrates with 0.15 kW radio frequency power and 0.55 Pascal gas pressure of argon inside the RF chamber for 12 min. The prepared ZnO seed layer over the glass substrates was annealed in a tubular furnace at 380°C under an atmosphere for 90 min in order to relieve the pressure on the coated layers.

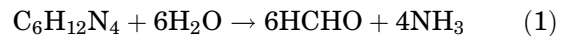
### Modified CBD Growth Process

High-quality vertically aligned ZnO NRs were synthesized using the modified chemical bath deposition method (Fig. 1). Deionized water was employed as the solvent and both HMTA and ZNH were used as precursors.

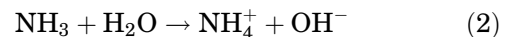
Equimolar 1:1 of both ( $\text{Zn}(\text{NO}_3)_2 \cdot 6\text{H}_2\text{O}$ ) and ( $\text{C}_6\text{H}_{12}\text{N}_4$ ), being 50 m Mol, were separately

dissolved in deionized water, and the dissolved solutions mixed with each other using a magnetic stirrer to obtain a homogenous growth solution. The pH value (initial pH) of the original growth solution was 6.7, and the growth solution was transparent. To investigate the effect of different growth temperatures on the ZnO NRs, the growth temperatures used were 65°C, 75°C, 85°C, 95°C, 105°C, and 115°C. The corresponding samples were labeled a, b, c, d, e, and f, respectively. The initial and final pH values of the growth solution were precisely measured before and after the growth process. The annealed ZnO seed layer-coated glass substrates were inserted inside a beaker at 70°C containing a mixture of the two growth solutions. To study the impact of the different growth temperatures on the ZnO NR properties, the CBD arrangement (beaker with seeded substrate and solution) were placed inside an oven under air bubbling with a 5000-mL/min flow rate and 70,000-Pascal air pressure for 180 min at 95°C. After finishing the required time of the growth process, the prepared ZnO NRs were washed using deionized water to remove all the remaining salt, and nitrogen gas was utilized to dry them. The main chemical reactions that describe the growth of the ZnO NRs are the following reactions:

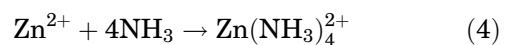
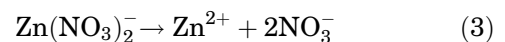
Decomposition reaction:



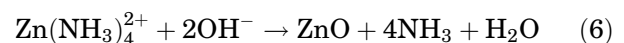
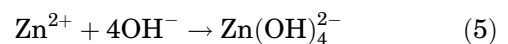
Hydroxyl supply reaction:



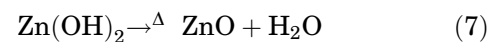
The formation of ZnO takes place with zinc nitrate hexahydrate-based solution:



Supersaturation reaction:



ZnO growth reaction:



### Characterization Techniques

The direct current (DC)/R sputtering system was an Auto HHV 500 sputter coater model, which was employed to coat the ZnO seed layer on the glass substrates. In addition, 1an annealing tube furnace model (Lenton VTF/12/60/700) was utilized to anneal the ZnO seed layer. A high-quality pH meter (PHSJ-4F; Hinotek) was utilized to measure the pH

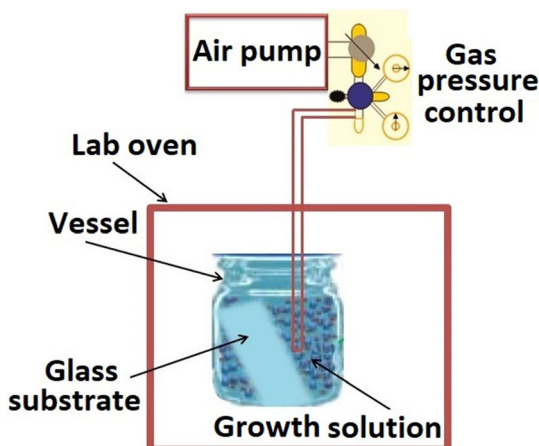


Fig. 1. Schematic of the modified CBD process.

of the growth solution, and three standard buffer pH solutions (pH 4, pH 7, and pH 10) were used to calibrate the meter. Field-emission scanning electron microscopes (FE-SEM) (FEI Nova; a nano-SEM 450, Netherlands, and a Leo-Supra 50 VP, Carl Zeiss, Germany) were used to examine and characterize the surface morphology, such as the top view and side view (cross-section, length, diameter, homogeneity, thickness, density, and distribution) and energy-dispersive x-ray spectroscopy (EDX) analysis provided (quantitative and qualitative) analyses of the elemental composition of the produced ZnO NRs. Also, the x-ray pattern and crystal structure (stress, strain, and quality of the epitaxial growth) of the ZnO NRs on the glass substrates were examined by using a high-resolution x-ray diffraction (XRD) system (X-Pert Pro MRD), with CuK $\alpha$  ( $\lambda = 0.154050$  nm) radiation and scanning range of  $2\theta$  set between  $20^\circ$  and  $80^\circ$ . In addition, a double-beam UV visible (UV-4100) spectrometer with a wavelength range 300–800 nm was utilized to characterize the optical properties and the  $E_g$  of the ZnO NR samples which were calculated from the transmittance spectrums of ZnO NR samples.

## RESULTS AND DISCUSSION

### ZnO NRs Top and Cross-Section View

To investigate the effect of growth temperature on the ZnO NRs, several samples were synthesized at different temperatures from  $65^\circ\text{C}$  to  $115^\circ\text{C}$ . The evolution of the morphology of the top and cross-sectional views of the samples were measured by using FE-SEM, as shown in Fig. 2. At the lower growth temperature of  $65^\circ\text{C}$ , it was observed that the ZnO NRs formed with a nonhomogeneous distribution and very low density on the entire glass substrate, while at higher temperatures up to  $95^\circ\text{C}$ , the growth of the NRs were with a homogeneous distribution and were hexagonal in shape, which was expected due to the wurtzite structure nature of the ZnO NRs, and, also, the NRs were oriented along the  $c$ -axis [0001] direction on the seeded substrate. Despite that, the ZnO NRs, generally, at different growth temperatures, produced non-uniform NRs in shape, size, and growth direction, and this aspect could be related to the starting of the nucleation process on the substrate.<sup>30</sup> Since the nucleation process does not happen simultaneously all over the substrate, some NRs will start growing earlier than the others, resulting in dispersion in the height and diameter of the NRs.<sup>31</sup> Bidier et al.<sup>32</sup> showed that Ti-doped ZnO NR arrays can be grown effectively onto Si substrates using the CBD method at  $93^\circ\text{C}$ . Pourshaban et al.<sup>33</sup> stated that the seed layer properties have a great impact on the nucleation, growth, and final properties of ZnO NR arrays.

Based on the FE-SEM analysis, Fig. 2, the average values of diameters, growth rates, and aspect ratios of the NRs are summarized in Fig. 3. The

average diameter dependence on the growth temperature is shown in Fig. 3a. It was observed that the average diameter of the ZnO NRs is reduced as the growth temperatures increased from  $65^\circ\text{C}$  to  $75^\circ\text{C}$ . This is, perhaps, due to the fact that the nucleation and growth are relatively slow in this range of temperature.<sup>11</sup> Conversely, the average diameter of the ZnO NRs gradually increased as the growth temperatures increased up to  $105^\circ\text{C}$ , and then sharply increased as the temperatures reached  $115^\circ\text{C}$ . Increasing the average diameter of ZnO NRs with growth temperatures may be due to the enhancement of the kinetics of the growth supporting the quick precipitation of ZnO add-atoms, resulting in a larger size of ZnO NRs.<sup>17</sup> This indicates that increasing the temperature would improve the aggregation and accelerate the reactive nucleation add-atoms during the solvothermal synthesis.<sup>34</sup> On the other hand, at higher growth temperatures, the adjacent ZnO NRs appear to merge with each other, producing new ZnO NRs with larger crystal sizes.<sup>35</sup>

Figure 3b shows the growth rate behavior with different growth temperatures. The growth rate of the ZnO NRs is gradually increased as the growth temperature increases from  $65^\circ\text{C}$  to  $95^\circ\text{C}$ . Thereafter, it is largely decreased at  $105^\circ\text{C}$  and  $115^\circ\text{C}$ . The maximum growth rate of the ZnO NRs in this study was obtained at  $95^\circ\text{C}$  and it was about 10.31 nm/min. Hence, the growth rate of the NRs along the  $c$ -axis (polar surface) will be much faster than along the radial axis (non-polar surface) with increasing growth temperature.<sup>36</sup> Also, it is clear from the SEM figures that the growth temperatures have clear influences on the growth rate of the individual faces of the crystals, as well as on the crystal dispensability. In a typical chemical bath deposition, the precursors are gradually depleted with time, and a higher reaction temperature leads to a faster depletion rate of the reactants. Therefore, as the solvent concentration decreases, the growth rate of the NR sidewalls diminishes significantly, resulting in a thinner tip and eventually a tapered structure.<sup>37</sup> Similar behaviors of ZnO NRs with different growth temperatures have also been reported by previous studies.<sup>38</sup>

The variation of aspect ratio of ZnO NRs with growth temperatures is displayed in Fig. 3c. The aspect ratio (length/diameter) of the ZnO NRs is gradually increased as the growth temperature increases from  $65^\circ\text{C}$  to  $95^\circ\text{C}$ , whereas increasing the growth temperature further from  $105^\circ\text{C}$  to  $115^\circ\text{C}$  causes the aspect ratio to rapidly drop. This is due to variation in the average length per diameter of the ZnO nanorods. This, perhaps, means that the highest aspect ratio is due to the smallest average diameter compared to the average length. The aspect ratios of ZnO nanorods for different growth temperatures have been investigated by numerous researchers.<sup>39</sup> It can be seen from Fig. 3c that the optimum growth temperature

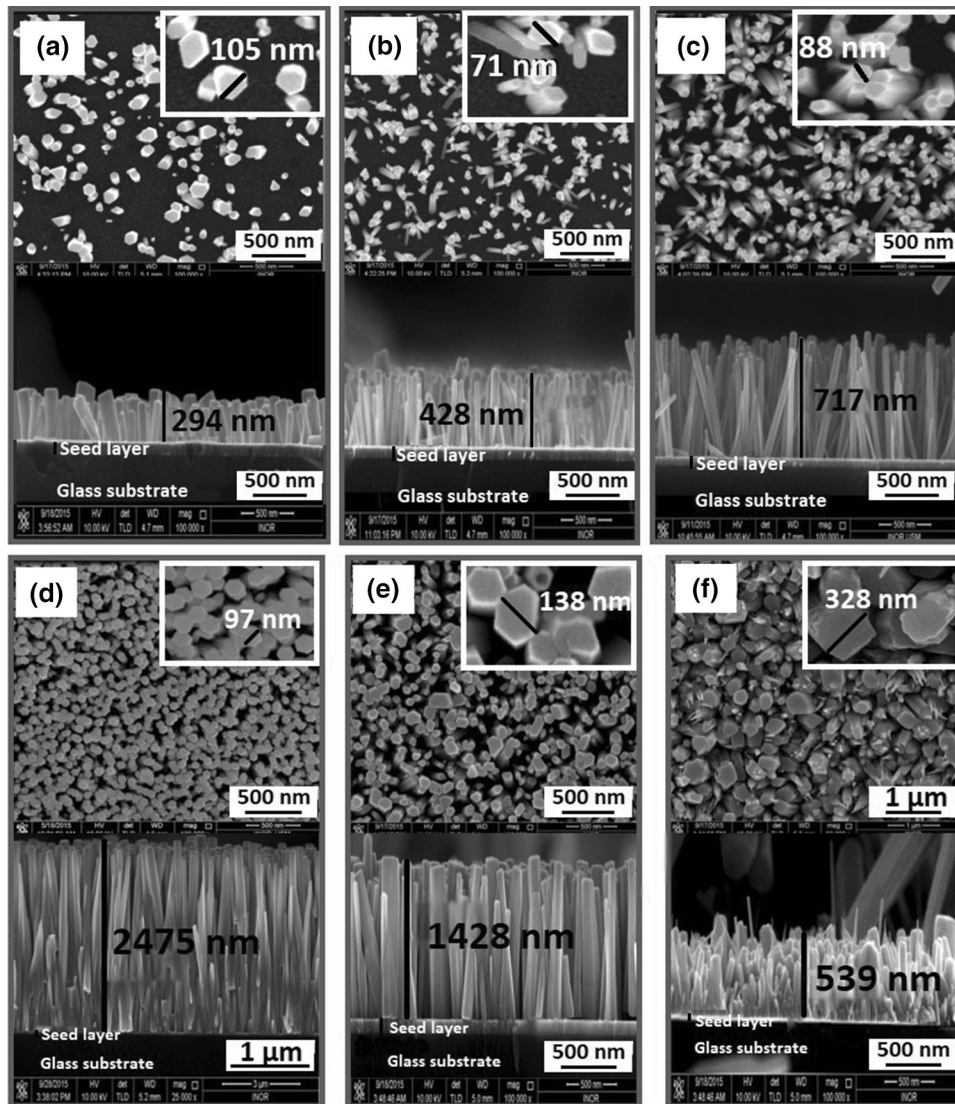


Fig. 2. Top and cross-section view FE-SEM images of ZnO nanorods for different growth temperatures: (a) 65°C, (b) 75°C, (c) 85°C, (d) 95°C, (e) 105°C, and (f) 115°C.

is 95°C due to having the highest aspect ratio, up to 25, compared to the other growth temperatures. A high aspect ratio is important for NRs as this feature plays a key factor in determining the energy conversion efficiency of solar cells and piezoelectric potential devices.<sup>40</sup> The high aspect ratio implies the more important impact of growth temperature on the longitudinal growth of ZnO NRs in the *c*-axis direction.<sup>41</sup>

### pH Value Discrepancy

The impact of growth temperature on the pH values in temperature ranges between 65°C and 115°C is shown in Fig. 4. The pH values are measured very carefully during the growth process. It can be seen from Fig. 4 that the final pH of the growth solution is gradually decreased with increasing the growth temperature. This is, most likely,

due to the fact that the increasing temperature is resulting from an increase in the thermal energy ( $k_B T$ ) of the solution and thus enhancing the molecular vibrations.<sup>42</sup> In the beginning, with a rising temperature, the observable  $H^+$  normally increases due to decreasing the affinity of the hydrogen bonds forming, which leads to the reduction of the pH values.<sup>43</sup> It can be noticed that the variation of the final pH value is quite small compared to the initial pH values. The growth process of the NRs can be considered as a competition between the growth temperature rate and the dissolution rate present in the solution.<sup>39</sup> The significant factor regarding the effect of growth temperatures is the solubility of ammonia ( $NH_3$ ) in the aqueous solutions, which can be significantly reduced at higher temperatures.<sup>44</sup> It can be stated that Eq. 8 has a crucial role in the ZnO NR formation.<sup>44</sup> At high temperature, i.e., more than

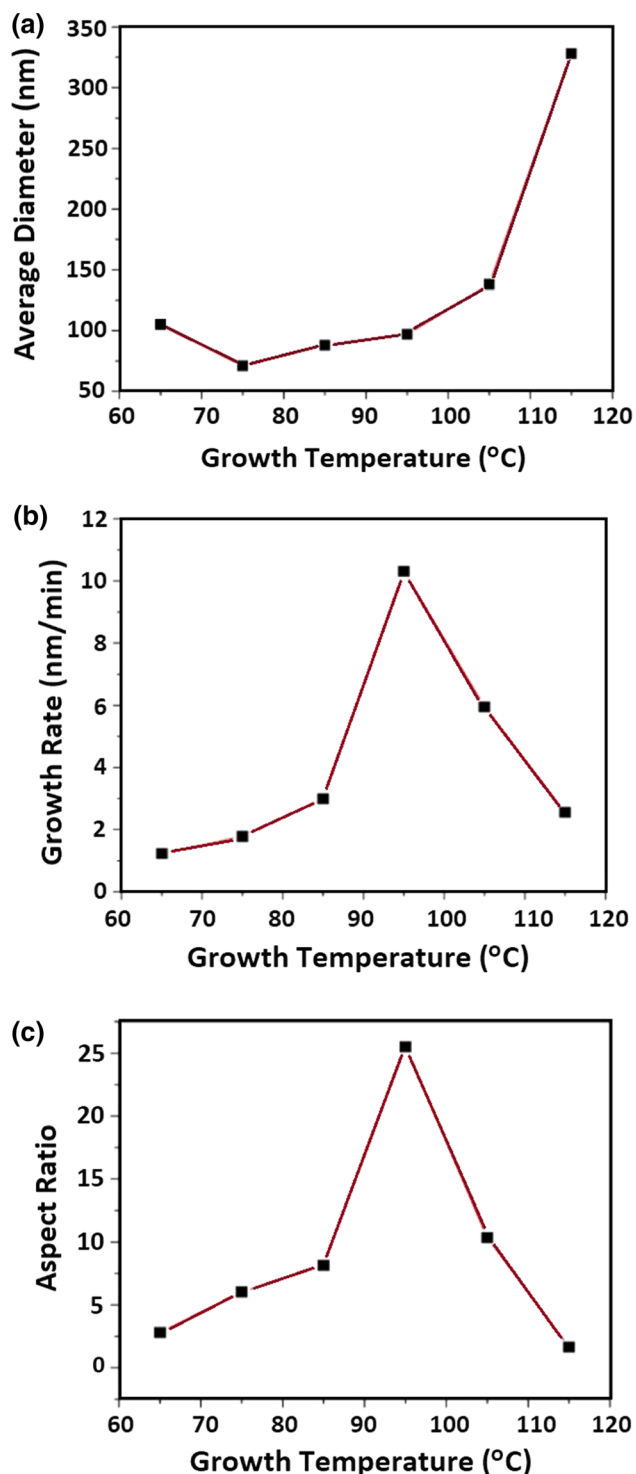


Fig. 3. Effect of different growth temperatures on the ZnO NRs: (a) average diameter, (b) average growth rate, (c) aspect ratio.

100°C, according to Eq. 2, water is donating one of its protons to ammonia. After the proton donation, the water turns into hydroxide, OH<sup>-</sup>. In this reaction, the water is acting as a Brønsted–Lowry acid. Ammonia accepts a proton from the water to form an ammonium ion, NH<sub>4</sub><sup>+</sup>. Therefore, ammonia is acting as a Brønsted–Lowry base. Thus, in the

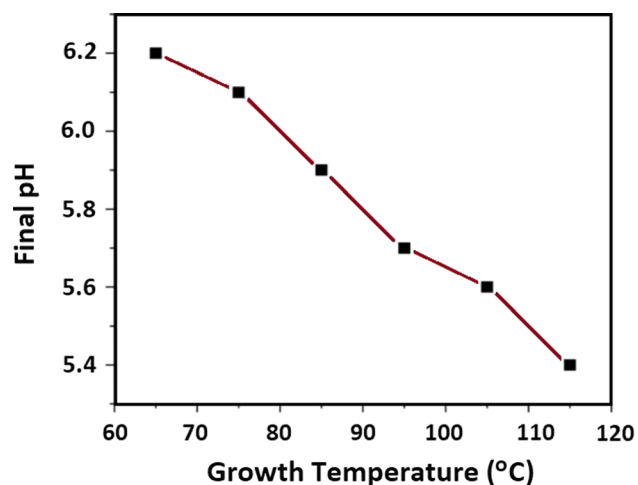
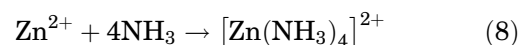


Fig. 4. Effect of different growth temperatures on the final pH values of the growth solution.

presence of low (OH<sup>-</sup>), the ZnO NRs will not growing properly due to insufficient Zn (OH)<sub>2</sub> formation, and the overall effects prevent the growth process. Accordingly, the final pH of the growth solution at the end of the reaction is decreased, followed by reductions of the average length and the growth rate of the ZnO NRs.<sup>45</sup>



Moreover, the growth rate and aspect ratio are displayed in Fig. 5, from which it can be seen that the growth rate and aspect ratio show a similar trend, and they are dramatically increasing with increasing pH value from 5.4 to 5.7. After that, a sharply decrease in the growth rate and aspect ratio can be seen as the pH values extend from 5.9 to 6.2. The highest aspect ratio is found at a value of the final pH of 5.7. This implies that, at higher values of the final pH of the growth solution, the length and growth rate of the ZnO NRs are reducing. In a similar study, Rafaie et al.<sup>46</sup> investigated the effect of pH during sol–gel synthesis of ZnO NRs using *Citrus aurantifolia* juice extracts.

### Energy Dispersive X-ray Spectroscopy (EDX) Analysis

The elemental chemical compositions of ZnO NRs at different growth temperatures were examined using EDX analysis. Figure 6 shows the EDX elemental mapping of nanorod arrays on the glass substrate corresponding to Zn and O, respectively, without the presence of any other impurities or substrate signals according to EDX limitations.

The stoichiometric ratio of Zn/O in the ZnO NRs is approximately 1:1. It is clear that the presence of Zn and O is uniform along the glass substrate (Fig. 7). The elemental mapping confirms that high-purity ZnO is formed along the glass substrate. The ratio between Zn and O was the same for all the analyzed

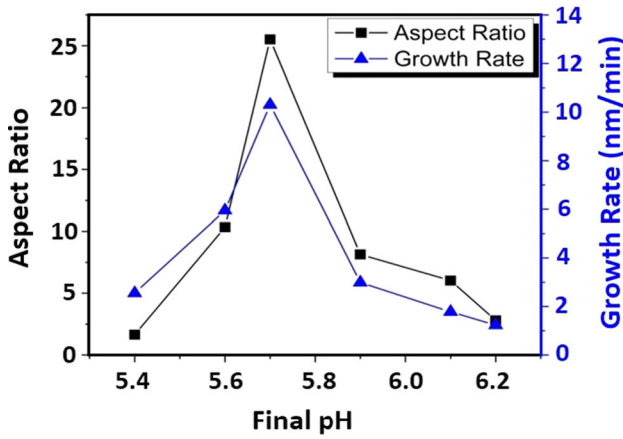


Fig. 5. Final pH versus growth rate and aspect ratio of ZnO NRs.

samples grown at different temperatures from 65°C to 115°C on the glass substrates. It can also be seen from Fig. 6 that the growth temperature has a durable impact on the ratio of Zn and O. From our view point, the increasing concentration of Zn, associated with a decreasing concentration of oxygen with increasing temperature, to a certain extent is related to the growth rate, which has been discussed previously (Fig. 3b). The maximum concentration of Zn can be obtained at 95°C, and it was about 55% (Fig. 7). Thus, it can be stated that the growth rate of the NRs along the *c*-axis will lead to the increasing the concentration of Zn with increasing growth temperature.<sup>47</sup> Afterward, the concentration of Zn starts to decrease at 105°C and 115°C to give a similar trend to that in Fig. 3b once again.

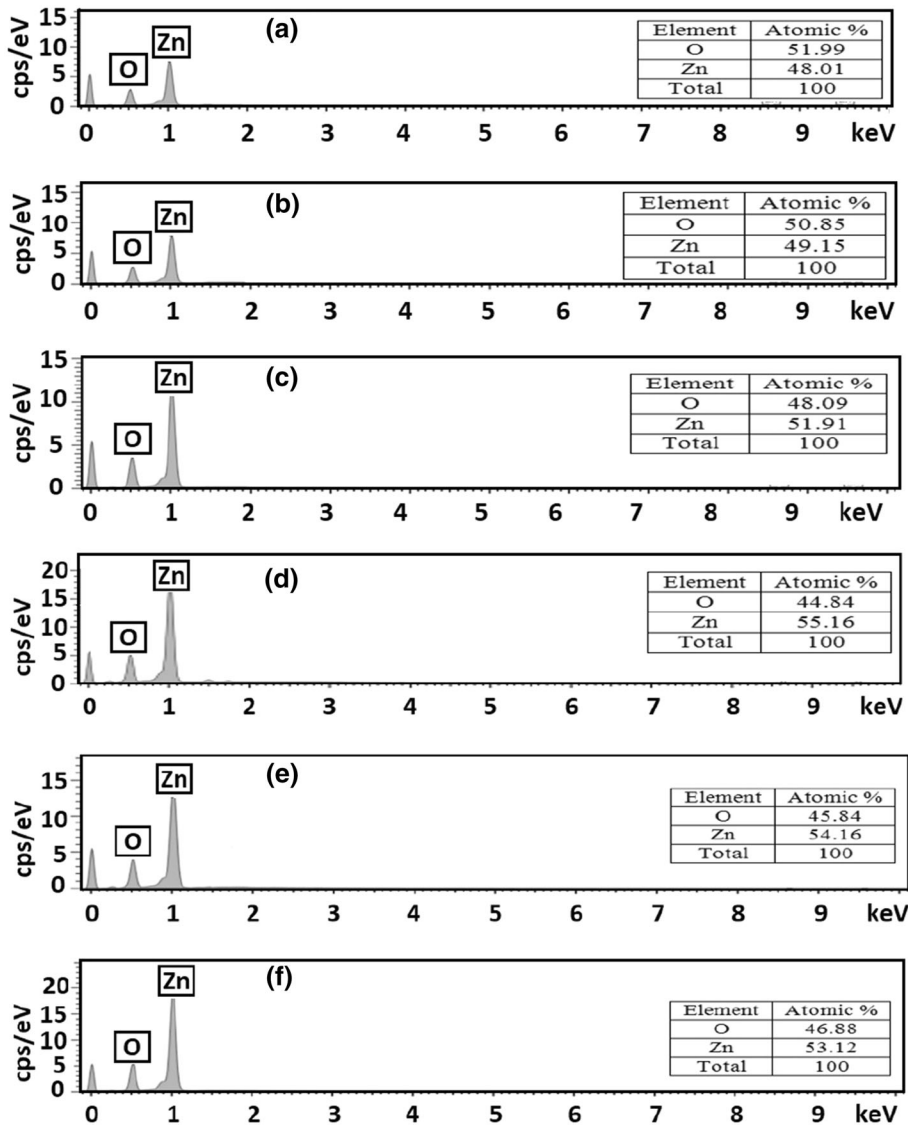


Fig. 6. EDX analysis of ZnO NRs for different growth temperatures: (a) 65°C, (b) 75°C, (c) 85°C, (d) 95°C, (e) 105°C, and (f) 115°C.

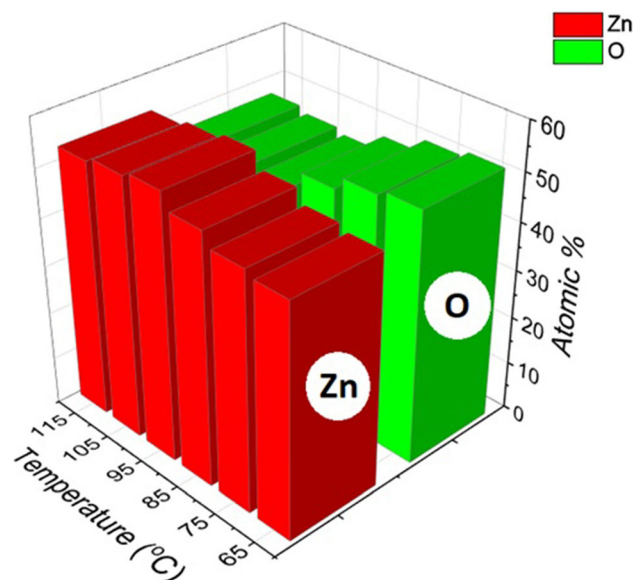


Fig. 7. Zn and O atomic % ratios of ZnO NRs using the data from Fig. 6.

### X-ray Diffraction Analysis

The x-ray diffraction patterns of ZnO NRs grown on the seeded substrates at different growth temperatures are displayed in Fig. 8. All the XRD diffraction peaks have been indexed as hexagonal crystal structure (wurtzite) of ZnO in accordance with JCPDS cards No. 01-080-0074. In addition, no other diffraction peaks from impurities or defects have been observed, confirming the high purity of the ZnO nanocrystals. In all the ZnO samples, the peaks at  $2\theta = 34.4^\circ$  and  $34.3^\circ$  correspond to the (002) plane. This verifies the preferential oriented growth along the  $c$ -axis as a result of possessing high kinetic energy. Therefore, it plays a crucial role in the column growth compared to the other planes, such as the (100) and (101) planes which have lower energy.<sup>48</sup> The strong and sharp (002) diffraction peak of the XRD patterns is also proving the high quality of the ZnO NRs synthesized along the  $c$ -axis and perpendicular to the glass substrate.<sup>49</sup> Figure 8-a reveals the semi-amorphous patterns for ZnO NRs formed at  $65^\circ\text{C}$ , which are in good agreement with the morphology characteristics, and the diffraction peak (100) is the dominant peak. It is believed that, at lower growth temperatures, there is insufficient thermal energy within the system, and therefore few of the atoms were arranged along the  $c$ -axis and most of them were moving away from the (002) orientation for the ZnO crystal, leading to non-uniform orientation along the  $c$ -axis.<sup>50</sup> As the growth temperature increased from  $75^\circ\text{C}$  to  $115^\circ\text{C}$ , the thermal energy adsorption by the molecules is quite enough to minimize the surface energy of the (002) plane. The existence of other diffraction peaks, such as (100), (101), (102), (110), (103), and (112), indicate that the NRs are not only nucleate on polar  $c$ -planes of the crystallites but also on the other

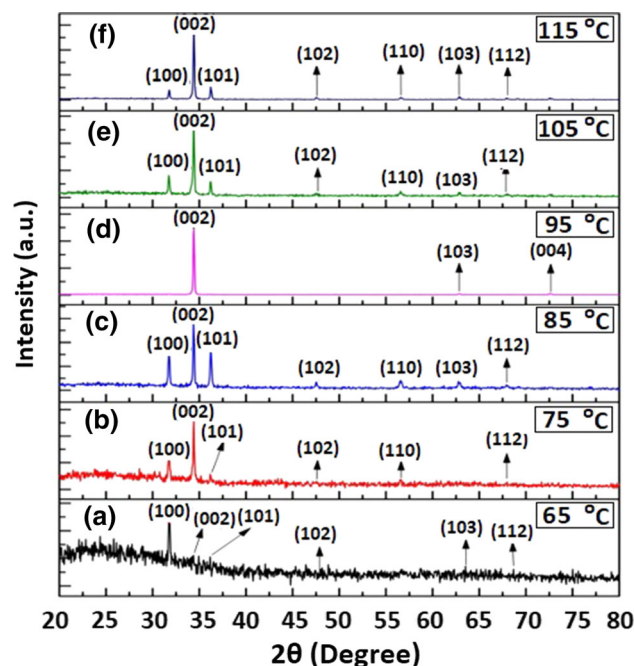


Fig. 8. X-ray diffraction patterns of ZnO NRs for different growth temperatures: (a)  $65^\circ\text{C}$ , (b)  $75^\circ\text{C}$ , (c)  $85^\circ\text{C}$ , (d)  $95^\circ\text{C}$ , (e)  $105^\circ\text{C}$ , and (f)  $115^\circ\text{C}$ .

nonpolar plane directions.<sup>51</sup> Similar XRD trends have been found by other researchers.<sup>52</sup> It is worth mentioning that the intensity of plane (002) becomes higher and narrower with increasing the growth temperature. This is, most probably, due to the atoms of the ZnO structure that gain more energy to rearrange themselves in the lattice and recrystallize at higher growth temperatures.<sup>53</sup> In addition, the NRs are well aligned with  $c$ -axis and are perpendicular on the substrate. This explains why the peak intensity improves more at higher growth temperatures. There is a strong correlation between the XRD results and the SEM morphology, especially when the growth temperature is  $95^\circ\text{C}$ .

The structural properties, peak position ( $\theta$ ), intensity, lattice constants ( $a$  and  $c$ ), and the internal strains ( $\epsilon_c$ ,  $\epsilon_a$ ) of the ZnO NRs along the diffraction peak (002) of different growth temperatures are listed in Table I. The lattice constants ( $a$  and  $c$ ) of the ZnO hexagonal structure are obtained using Bragg's law<sup>54</sup>:

$$a = \sqrt{\frac{1}{3}} \frac{\lambda}{\sin \theta} \quad (9)$$

$$c = \frac{\lambda}{\sin \theta} \quad (10)$$

where  $\lambda$  is the wavelength of the x-ray source and  $\theta$  is the angle of the diffraction peak.

The strains ( $\epsilon_c$ ) and ( $\epsilon_a$ ) of the ZnO along the  $a$ -axis and the  $c$ -axis, respectively, are calculated from the following equations<sup>54</sup>:



**Table I. Lattice parameters and structure properties of ZnO NRs of diffraction peak (002) and (100) planes for different growth temperatures**

Growth temperature (°C)	Plane	2θ	I (a.u)	a (Å)	c (Å)	ε <sub>a</sub> %	ε <sub>c</sub> %	d (Å)
65	100	31.77	92	3.2491	5.627	7.913	- 0.132	2.813
75	002	34.38	182	3.0093	5.212	- 7.505	- 0.053	2.606
85	002	34.39	406	3.0087	5.211	- 7.523	- 0.073	2.605
95	002	34.40	3206	3.0078	5.209	- 7.550	- 0.102	2.604
105	002	34.37	510	3.0099	5.213	- 7.487	- 0.034	2.606
115	002	34.36	1782	3.0109	5.215	- 7.457	- 0.002	2.607

$$\varepsilon_a = \frac{a - a_o}{a_o} \times 100\% \quad (11)$$

$$\varepsilon_c = \frac{c - c_o}{c_o} \times 100\% \quad (12)$$

where  $a_o$  and  $c_o$  represent the standard lattice constants for unstrained ZnO NRs which exist in the database.<sup>55</sup> The difference of strains ( $\varepsilon_c$ ) and ( $\varepsilon_a$ ) as displayed in Table I is due to the variation in the values of interplaner spacing as a result of a mismatch between crystal growth and the substrate. The lowest strains along the ZnO NRs (002) peak are obtained when the growth temperature is 95°C. A negative value of strain is associated with compressive strain and represents the lattice contraction, while a positive value of strain is related to tensile strain, specifying the expansion in the lattice constant.<sup>15</sup>

The interplaner distance of ZnO nanorods along the (002) peak has been found according to Bragg's law,<sup>15</sup> and its results are summarized in Table I.

$$\frac{1}{d^2} = \frac{4}{3} \left( \frac{h^2 + hk + k^2}{a^2} \right) + \frac{l^2}{c^2} \quad (13)$$

where  $d$  is the lattice plane spacing and  $h$ ,  $k$ ,  $l$  are Miller indices from the XRD peaks.

The maximum and minimum interplaner distance of the prepared ZnO NRs at different growth temperatures along the (002) peaks are observed at the temperatures of 115°C and 95°C, respectively. This may be due the peak position value  $2\theta$  along the (002) peaks.

It is clear that the average crystalline size of ZnO NRs along the diffraction peaks (002) are strongly influenced by growth temperatures from 75°C to 115°C, which are calculated by using the Debye-Scherrer formula<sup>56</sup>:

$$D = \frac{k\lambda}{\beta \cos \theta} \quad (14)$$

where  $k$  is a constant which is taken to be 0.9,  $\lambda$  is the wavelength of the x-ray source,  $\beta$  is full width at half maximum (FWHM) measured in radians, and  $\theta$  is the Bragg diffraction angle.

The crystal size of ZnO NRs is increased sharply as the growth temperature increases from 75°C to

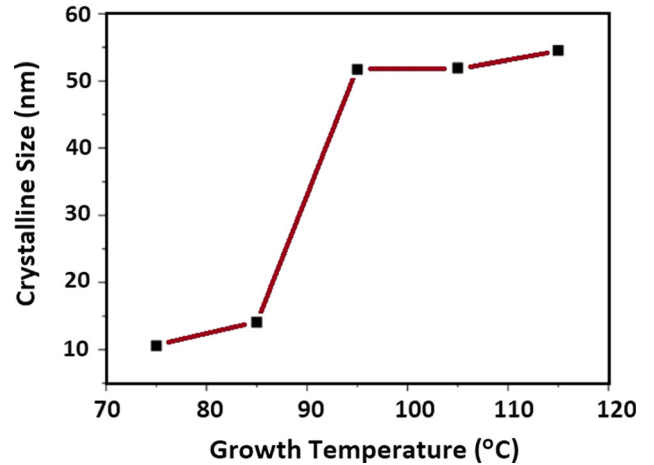


Fig. 9. Effect of different growth temperatures on crystalline size of ZnO NRs of diffraction peak (002).

95°C, and then it is increased slightly beyond 95°C, as shown in Fig. 9. The obtained crystalline size results of ZnO NRs are in good agreement with the previous studies.<sup>57</sup>

The FWHM and dislocation density of ZnO NRs of (002) diffraction peaks are given in Fig. 10. The FWHM is decreased with growth temperatures from 75°C to 115°C, signifying the improvement in the crystal quality. The minimum value of FWHM is observed when the ZnO NRs are grown at 95°C.

The dislocation density ( $\delta$ ), which represents the amount of defects originated from the internal strain and mismatch between the substrate and crystal growth, is calculated by the following equation:<sup>58</sup>

$$\delta = \frac{1}{D^2} \quad (15)$$

where  $D$  is the crystallite size.

The dislocation density (Fig. 10) is continuously decreased as the growth temperature increases from 75°C to 115°C. This indicates a reduction in the number of defects in the crystal growth at higher temperatures.<sup>59</sup> Additionally, the dislocation density is inversely proportional to the square of the crystal size due to the increase in the crystalline size with growth temperature. These results are in good agreement with the previous work.<sup>58,60</sup>

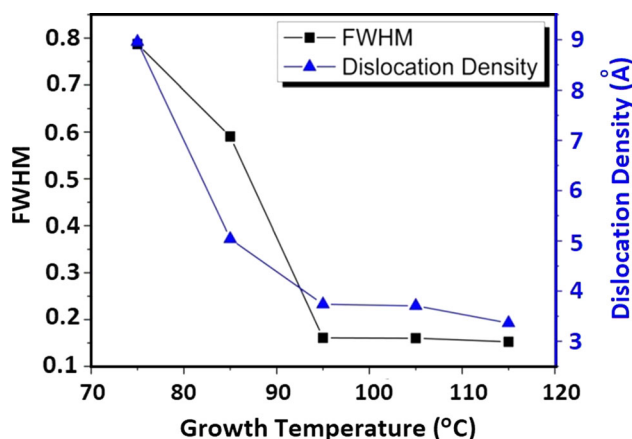


Fig. 10. Effect of different growth temperatures on the FWHM and dislocation density of ZnO NRs of (002) diffraction peaks.

Likewise, the effect of the different growth temperatures on the bond length and volume of the hexagonal cells of ZnO are shown in Fig. 11, calculated by the following equation<sup>61</sup>:

$$L = \sqrt{\frac{a^2}{3} + \left(\frac{1}{2} - u\right)^2 c^2} \quad (16)$$

where  $u$  is a parameter related to the  $c/a$  ratio, and  $u$  is a measurement of the amount of each atom displaced with respect to the next one along the  $c$ -axis, and is given by the following formula<sup>61</sup>:

$$u = \frac{a^2}{3c^2} + 0.25 \quad (17)$$

Also, the volume of the hexagonal cell ( $V$ ) has been evaluated by the following formula<sup>61</sup>:

$$V = \frac{\sqrt{3}}{2} a^2 c \quad (18)$$

It can be seen from Fig. 11 that the bond length and the volume of ZnO NRs have almost similar tendencies. Both are gradually decreased with growth temperature from 75°C to 95°C, and then suddenly increased with further growth temperature from 95°C to 115°C. This variation of the volume and the bond length is due to a diversity in the peak position  $2\theta$  along the (002) plane since both are directly dependent on the lattice parameters  $a$  and  $c$ , and also on the value of  $2\theta$ . These results are in good agreement with previous studies.<sup>62</sup>

### Ultraviolet Visible (UV-Vis) Spectroscopy Analysis

In order to investigate the effect of different growth temperatures on the optical properties of ZnO NRs, UV visible spectroscopy has been used at RT based on the transmittance spectrums. Figure 12

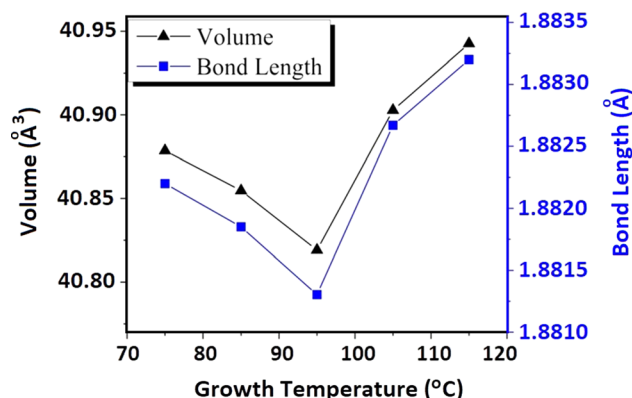


Fig. 11. Effect of different growth temperatures on the volume of hexagonal cell and bond length of ZnO NRs of diffraction peak (002).

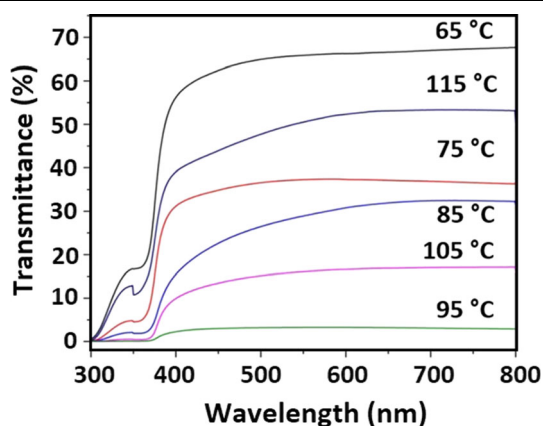


Fig. 12. Optical transmittance spectrum of ZnO NRs prepared at different growth temperatures.

shows the optical transmittance spectrum from the ZnO NRs at different growth temperatures from 65°C to 115°C. All the ZnO nanorods have low transmittance in the UV region, i.e.,  $\lambda < 400$  nm, and high transmittance in the visible region, i.e., between 400 and 600 nm. The average optical transmittance suddenly drops near UV region at a wavelength around 388 nm due to the corresponding optical absorption. From Fig. 12, a higher transmittance from ZnO NRs is observed at 65°C, which can be decreased sharply, from  $\sim 66\%$  to  $\sim 3.3\%$  as the growth temperature increases from 65°C to 95°C. This is, perhaps, due to the increase in the light scattering from voids, grains, and the ZnO film thickness grown at 95°C.<sup>63</sup> However, as the growth temperature increases from 95°C to 105°C and 115°C, the transmittance rapidly increases to  $\sim 16.5\%$  and  $\sim 53\%$ , respectively. This could be related to the reduction of dislocation density and average length of nanorods at higher temperatures.<sup>64</sup> Also, increasing the optical transmittance results in reducing the optical scattering and

absorption when the average crystal size and length of NRs are small, as can be observed clearly at the low temperature of 65°C.<sup>65</sup> In general, surface thickness, defects such as impurities, dislocation, and homogeneity of nanorod distribution are the main factors affecting the optical transmittance of the ZnO nanostructure.<sup>66</sup>

In this study, the decrease in the average transmittance of the fabricated ZnO nanorods as the growth temperatures increased could be related to two factors. First, ZnO NRs have a larger grain size and larger surface roughness at higher growth temperatures, as shown in Fig. 13. Second, the thicker ZnO NRs are producing higher absorption rates of the light. The absorption edge shifts towards longer wavelengths with increasing the growth temperatures from 65°C to 115°C. This is possibly related to the degree of crystallinity and the grain size of the structure.<sup>67</sup> These outcomes are in a good agreement with previous studies.<sup>49,68</sup>

The optical band gap energy of ZnO NRs fabricated at various growth temperatures was calculated through the transmittance spectra using the Tauc formula by the extrapolation of the linear portion of  $(\alpha h\nu)^2$  versus  $h\nu$ ,<sup>24</sup> as shown in Fig. 14.

$$(\alpha h\nu)^2 = A(h\nu - E_g)^n \quad (19)$$

where  $\alpha$  is the absorption coefficient,  $h\nu$  is the photon energy,  $A$  is a constant,  $E_g$  is the optical band gap energy, and  $n$  depends on the transmission type (equal to 1/2 for allowed direct transmission). Assuming a negligible reflectance, then Beer's law gives  $A = 2 - \log_{10} \%T$ ; where  $A$  the absorbance and  $\%T$  is the percentage transmission. After converting  $A$  into  $\%T$  spectrum, then  $\alpha$ , the absorption coefficient, can be calculated by<sup>22</sup>:

$$\alpha = \frac{\ln(\frac{1}{\%T})}{d} \quad (20)$$

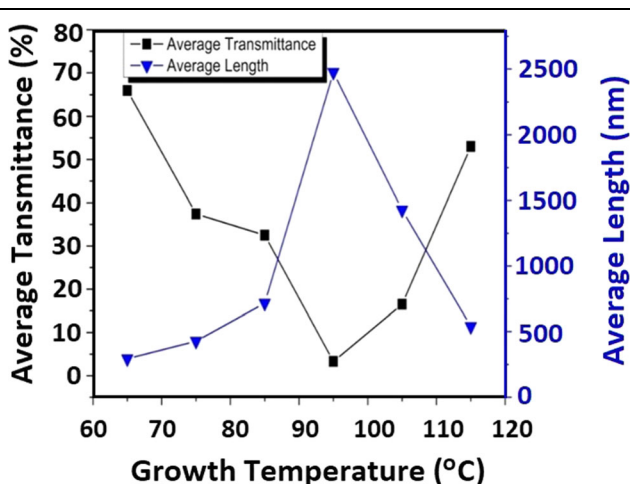


Fig. 13. Effect of different growth temperature on the average transmittance and average length of ZnO NRs.

where  $T$  is the transmittance of the ZnO films, and  $d$  is the film thickness. Accordingly, the tangent line at the linear part of the curve can give a good estimation of the band gap energy for this direct transition. From the plots, it can be observed that the transition region is around 3.2 eV, which corresponds to the direct transition between the edges of the valence and conduction bands that represent the energy band gap ( $E_g$ ) of the ZnO. The calculated values of the ZnO energy band gap are 3.24 eV, 3.23 eV, 3.19 eV, 3.15 eV, 3.195 eV, and 3.21 eV grown for different growth temperatures of 65°C, 75°C, 85°C, 95°C, 105°C, and 115°C, respectively. The band gap of a crystal structure can be governed by its crystalline quality, defect states, and crystal size.<sup>69</sup> The investigated energy band gap of ZnO NRs decreased as the growth temperatures increased from 65°C to 95°C, and then increased as the growth temperature increased from 95°C to 115°C. The decrease band gap energy as the growth temperatures increased is due to the crystal quality and larger crystal size at the higher temperature of 95°C.<sup>70</sup> On the other hand, the broadening in the energy band gap values with growth temperatures up to 115°C are attributed to the increase in the transition tail width as a result of higher compressive strain along the  $c$ -axis. The obtained energy band gap behavior for different temperatures are in a good agreement with previously reported studies.<sup>27,71</sup>

## CONCLUSIONS

High crystal quality and vertically-aligned ZnO NRs were successfully fabricated on glass substrates using a low-cost, low-temperature, and simple modified chemical bath deposition. The use of air bubbles in the growth solution during the CBD processes is an inimitable modified process. This investigation showed that the growth temperature has a significant impact on the synthesis of ZnO NRs. SEM and XRD studies indicated that the synthesized ZnO NRs possess a uniform hexagonal shape with a preferential growth direction along the [002] orientation. It was also noted that the aspect ratio (length/diameter) of the ZnO NRs increases with growth temperature up to 95°C and beyond that it started decreasing sharply. The average length ranged from 294 nm to 2475 nm, while the average diameter increased from 71 nm to 328 nm. The aspect ratio, in its turn, increases relatively more with the growth temperature. Moreover, the crystal qualities possess improved structural properties as displayed by the narrowing of the x-ray diffraction peaks on the polar surface  $c$ -axis with reducing dislocation density at higher growth temperatures. The highest optical transmittance spectrum of ZnO NRs was observed when the growth temperature was 65°C, while it decreased from ~66% to ~3.3% as the growth temperature increased from 65°C to 95°C. This is, conceivably, due to the light scattering increase from voids, grain size and

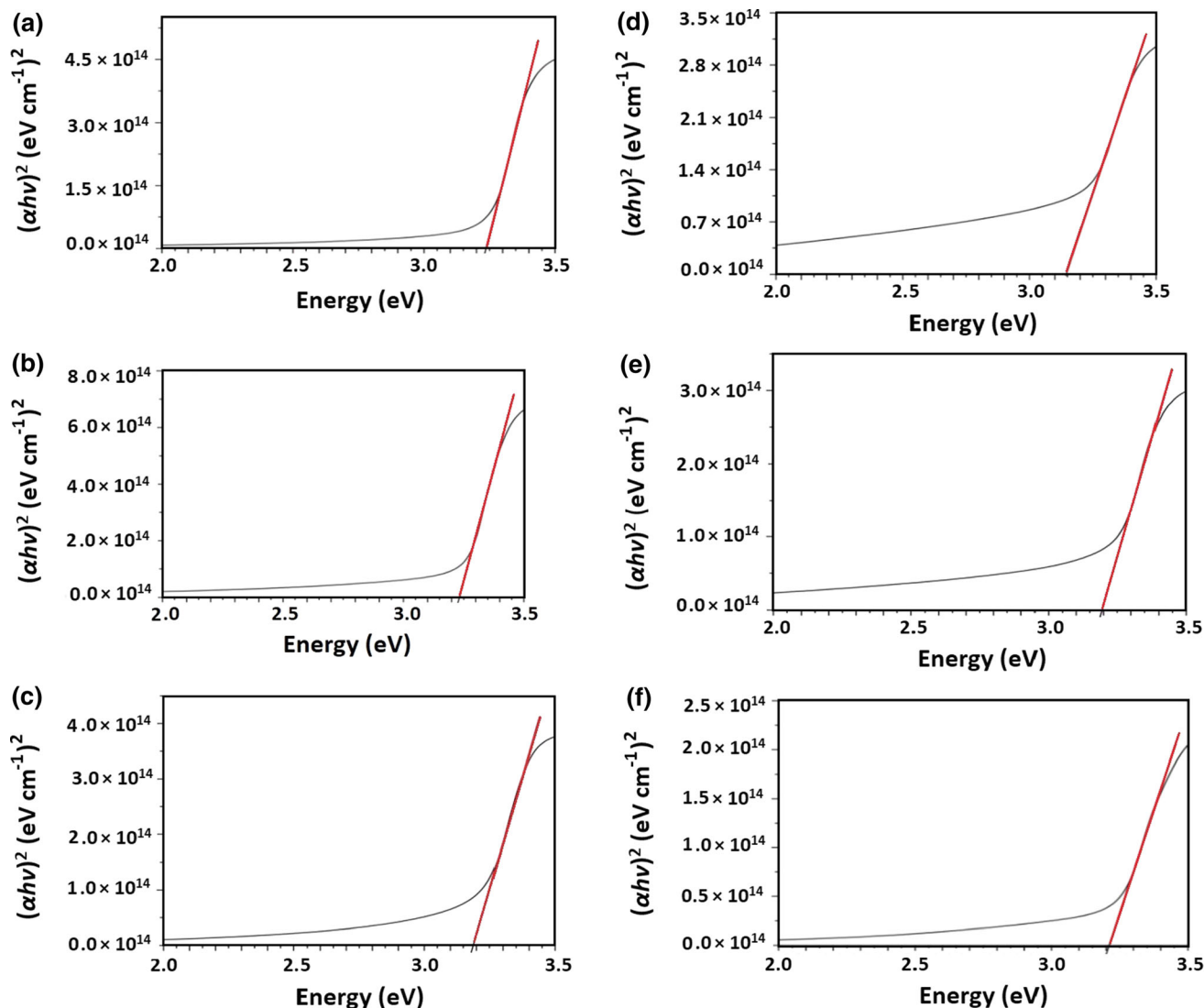


Fig. 14. Tauc plot  $(\alpha h\nu)^2$  versus photon energy  $(h\nu)$  of the ZnO nanorods for different growth temperatures: (a) 65°C, (b) 75°C, (c) 85°C, (d) 95°C, (e) 105°C, and (f) 115°C.

thickness of the ZnO NRs. The UV-Vis absorption spectrum indicated that the energy band gap decreased as the growth temperature increased from 65°C to 95°C. Then, the energy band gap increased with the growth temperature from 95°C to 115°C as a result of distortion of the crystal quality, crystal size, and internal strain through the ZnO NRs. Above and beyond, the chemical bath deposition method is more efficient and dependable owing to the advantages of its simple process and high product quality.

#### ACKNOWLEDGMENTS

The authors would like to thank Dr Mukhtar Ahmed at SISAF, Ulster University, UK, for his valuable assistance throughout this investigation. They also want to thank Dr. David M.W. Waswa at Tishk International University for his diligent proofreading of this manuscript.

#### CONFLICT OF INTEREST

The authors declare that they have no conflict of interest.

#### REFERENCES

1. M. Rasheed, and R. Barillé, M. Rasheed, and R. Barillé, *Opt. Quantum Electron.*, 2017, **49**, p 190.
2. M. Mickan, U. Helmersson, H. Rinnert, J. Ghanbaja, D. Muller, and D. Horwat, M. Mickan, U. Helmersson, H. Rinnert, J. Ghanbaja, D. Muller, and D. Horwat, *Sol. Energy Mater. Sol. Cells.*, 2016, **157**, p 742.
3. Z. Zhang, X. Li, H. Chen, G. Shao, R. Zhang, and H. Lu, Z. Zhang, X. Li, H. Chen, G. Shao, R. Zhang, and H. Lu, *Mater. Res. Express*, 2018, **5**, p 015021.
4. M. Girtan, M. Girtan, *Sol. Energy Mater. Sol. Cells.*, 2012, **100**, p 153.
5. S. Pearton, and F. Ren, S. Pearton, and F. Ren, *Curr. Opin. Chem. Eng.*, 2014, **3**, p 51.
6. S. Park, C. Hwang, M. Ryu, S. Yang, C. Byun, J. Shin, J. Lee, K. Lee, M. Suk Oh, and S. Im, S. Park, C. Hwang, M. Ryu, S. Yang, C. Byun, J. Shin, J. Lee, K. Lee, M. Suk Oh, and S. Im, *Adv. Mater.*, 2009, **21**, p 678.

7. M. Choi, D. Choi, M. Jin, I. Kim, S. Kim, J. Choi, S. Yoon Lee, J. Min Kim, and S. Kim, M. Choi, D. Choi, M. Jin, I. Kim, S. Kim, J. Choi, S. Yoon Lee, J. Min Kim, and S. Kim, *Adv. Mater.*, 2009, **21**, p 2185.
8. L. Zhu, and W. Zeng, L. Zhu, and W. Zeng, *Sens. Actuator A Phys.*, 2017, **267**, p 242.
9. S. Prakash Mondal, S. Dhar, and T. Majumder, in *Physical Chemistry for Chemists and Chemical Engineers* (Apple Academic, New York, 2018), p 117.
10. M. Ahmad, and J. Zhu, M. Ahmad, and J. Zhu, *J. Mater. Chem.*, 2011, **21**, p 599.
11. Q. Li, J. Bian, J. Sun, J. Wang, Y. Luo, K. Sun, and D. Yu, Q. Li, J. Bian, J. Sun, J. Wang, Y. Luo, K. Sun, and D. Yu, *Appl. Surf. Sci.*, 2010, **256**, p 1698.
12. B. Cao, W. Cai, Y. Li, F. Sun, and L. Zhang, B. Cao, W. Cai, Y. Li, F. Sun, and L. Zhang, *Nanotechnology*, 2005, **16**, p 1734.
13. M. De Guire, L. Pitta Bauermann, H. Parikh, and J. Bill, in *Chemical Solution Deposition of Functional Oxide Thin Films* (Springer, 2013), p 319.
14. T. Lee, H. Ryu, and W. Lee, T. Lee, H. Ryu, and W. Lee, *J. Alloys Compd.*, 2014, **597**, p 85.
15. A. Abdulrahman, S. Ahmed, N. Ahmed, and M. Almessiere, A. Abdulrahman, S. Ahmed, N. Ahmed, and M. Almessiere, *Dig. J. Nanomater. Biostruct. (DJNB)*, 2016, **11**, p 111.
16. J. Gomez, and O. Tigli, J. Gomez, and O. Tigli, *J. Mater. Sci.*, 2013, **48**, p 612.
17. G. Amin, M. Asif, A. Zainelabdin, S. Zaman, O. Nur, and M. Willander, G. Amin, M. Asif, A. Zainelabdin, S. Zaman, O. Nur, and M. Willander, *J. Nanomater.*, 2011, **2011**, p 123.
18. M. Kamruzzaman, and J. Zapfen, M. Kamruzzaman, and J. Zapfen, *Crystallogr. Rep.*, 2018, **63**, p 456.
19. A. Mebdir Holi, Z. Zainal, Z. Abidin Talib, H. Lim, C. Yap, S. Chang, and A. Kadim Ayal, A. Mebdir Holi, Z. Zainal, Z. Abidin Talib, H. Lim, C. Yap, S. Chang, and A. Kadim Ayal, *Optik*, 2016, **127**, p 11111.
20. R. Nandi, R. Srinivasa, and S. Major, R. Nandi, R. Srinivasa, and S. Major, *Mater. Chem. Phys.*, 2016, **182**, p 155.
21. S. Gawali, S. Mahadik, F. Pedraza, C. Bhosale, H. Pathan, and S. Jadhkar, S. Gawali, S. Mahadik, F. Pedraza, C. Bhosale, H. Pathan, and S. Jadhkar, *J. Alloys Compd.*, 2017, **704**, p 788.
22. S. Safa, A. Khayatian, and M. Najafi, S. Safa, A. Khayatian, and M. Najafi, *J. Adv. Mater. Process.*, 2015, **3**, p 49.
23. O. Farhat, M. Halim, N. Ahmed, and M. Qaeed, O. Farhat, M. Halim, N. Ahmed, and M. Qaeed, *Superlattices Microstruct.*, 2016, **100**, p 1120.
24. A. Abdulrahman, S. Ahmed, and M. Almessiere, A. Abdulrahman, S. Ahmed, and M. Almessiere, *Dig. J. Nanomater. Biostruct. (DJNB)*, 2017, **12**, p 1001.
25. Z. Zheng, J. Lin, X. Song, and Z. Lin, Z. Zheng, J. Lin, X. Song, and Z. Lin, *Chem. Phys. Lett.*, 2018, **712**, p 155.
26. A. Ghosh, D. Chaudhary, A. Biswas, R. Thangavel, and G. Udayabhanu, A. Ghosh, D. Chaudhary, A. Biswas, R. Thangavel, and G. Udayabhanu, *RSC Adv.*, 2016, **6**, p 115204.
27. R. Pietruszka, B. Sławomir Witkowski, S. Gieraltowska, P. Caban, L. Wachnicki, E. Zielony, K. Gwozdz, P. Bieganski, E. Placzek-Popko, and M. Godlewski, R. Pietruszka, B. Sławomir Witkowski, S. Gieraltowska, P. Caban, L. Wachnicki, E. Zielony, K. Gwozdz, P. Bieganski, E. Placzek-Popko, and M. Godlewski, *Sol. Energy Mater. Sol. Cells*, 2015, **143**, p 99.
28. V. Thanh Duoc, D. Thi Thanh Le, N. Duc Hoa, N. Van Duy, C. Manh Hung, H. Nguyen, and N. Van Hieu, V. Thanh Duoc, D. Thi Thanh Le, N. Duc Hoa, N. Van Duy, C. Manh Hung, H. Nguyen, and N. Van Hieu, *J. Nanomater.*, 2019, **2019**, p 122.
29. S. Goel, N. Sinha, H. Yadav, A. Joseph, and B. Kumar, S. Goel, N. Sinha, H. Yadav, A. Joseph, and B. Kumar, *Phys. E Low Dimens. Syst. Nanostruct.*, 2017, **91**, p 72.
30. L. Cui, G. Wang, H. Zhang, R. Sun, X. Kuang, and J. Han, L. Cui, G. Wang, H. Zhang, R. Sun, X. Kuang, and J. Han, *Ceram. Int.*, 2013, **39**, p 3261.
31. M. Firdaus Malek, M. Hafiz Mamat, T. Soga, S. Abdul Rahman, S. Abu Bakar, A. Syakirin Ismail, R. Mohamed, S. Alrokayan, H. Khan, and M. Rusop Mahmood, M. Firdaus Malek, M. Hafiz Mamat, T. Soga, S. Abdul Rahman, S. Abu Bakar, A. Syakirin Ismail, R. Mohamed, S. Alrokayan, H. Khan, and M. Rusop Mahmood, *Jpn. J. Appl. Phys.*, 2015, **55**, p 0115.
32. S. Bidier, M. Hashim, A. Al-Diabat, and M. Bououdina, S. Bidier, M. Hashim, A. Al-Diabat, and M. Bououdina, *Phys. E Low Dimens. Syst. Nanostruct.*, 2017, **88**, p 169.
33. E. Pourshaban, H. Abdizadeh, and M. Reza Golobostanfard, E. Pourshaban, H. Abdizadeh, and M. Reza Golobostanfard, *Ceram. Int.*, 2016, **42**, p 14721.
34. S. Shaziman, A. Syakirin Ismail, M. Hafiz Mamat and A. Sabirin Zoolfakar, in *IOP Conference Series, Materials Science and Engineering*, p. 012016 (2015).
35. V. Gaddam, R. Rakesh Kumar, M. Parmar, M. Nayak, and K. Rajanna, V. Gaddam, R. Rakesh Kumar, M. Parmar, M. Nayak, and K. Rajanna, *RSC Adv.*, 2015, **5**, p 89985.
36. A. Umar, C. Ribeiro, A. Al-Hajry, Y. Masuda, and Y. Hahn, A. Umar, C. Ribeiro, A. Al-Hajry, Y. Masuda, and Y. Hahn, *J. Phys. Chem. C.*, 2009, **113**, p 14715.
37. J. Zhao, X. Yan, Y. Lei, Y. Zhao, Y. Huang, and Y. Zhang, J. Zhao, X. Yan, Y. Lei, Y. Zhao, Y. Huang, and Y. Zhang, *Adv. Mater. Res.*, 2012, **1**, p 75.
38. J. Yang, J. Lang, L. Yang, Y. Zhang, D. Wang, H. Fan, H. Liu, Y. Wang, and M. Gao, J. Yang, J. Lang, L. Yang, Y. Zhang, D. Wang, H. Fan, H. Liu, Y. Wang, and M. Gao, *J. Alloys Compd.*, 2008, **450**, p 521.
39. K. Gurav, M. Gang, S. Shin, U. Patil, P. Deshmukh, G. Agawane, M. Suryawanshi, S. Pawar, P. Patil, and C. Lokhande, K. Gurav, M. Gang, S. Shin, U. Patil, P. Deshmukh, G. Agawane, M. Suryawanshi, S. Pawar, P. Patil, and C. Lokhande, *Sens. Actuators B Chem.*, 2014, **190**, p 439.
40. R. Ahmad, N. Tripathy, M. Ahn, and Y. Hahn, R. Ahmad, N. Tripathy, M. Ahn, and Y. Hahn, *Sci. Rep.*, 2017, **7**, p 46475.
41. Y. Qu, X. Huang, Y. Li, G. Lin, B. Guo, D. Song, and Q. Cheng, Y. Qu, X. Huang, Y. Li, G. Lin, B. Guo, D. Song, and Q. Cheng, *J. Alloys Compd.*, 2017, **698**, p 719.
42. R. Wahab, S. Ansari, Y. Soon Kim, M. Song, and H. Shin, R. Wahab, S. Ansari, Y. Soon Kim, M. Song, and H. Shin, *Appl. Surf. Sci.*, 2009, **255**, p 4891.
43. S. Baruah, and J. Dutta, S. Baruah, and J. Dutta, *J. Cryst. Growth*, 2009, **311**, p 2549.
44. S. Wang, T. Tseng, Y. Wang, C. Wang, H. Lu, and W. Shih, S. Wang, T. Tseng, Y. Wang, C. Wang, H. Lu, and W. Shih, *Int. J. Appl. Ceram. Technol.*, 2008, **5**, p 419.
45. N. Harale, A. Kamble, N. Tarwal, I. Mulla, V. Rao, J. Kim, and P. Patil, N. Harale, A. Kamble, N. Tarwal, I. Mulla, V. Rao, J. Kim, and P. Patil, *Ceram. Int.*, 2016, **42**, p 12807.
46. H. Rafeaie, N. Samat, and R. Md Nor, H. Rafeaie, N. Samat, and R. Md Nor, *Mater. Lett.*, 2014, **137**, p 297.
47. T. Nguyen, N. Tuan, N. Cuong, N. Kien, P. Huy, V. Hieu Nguyen, and D. Nguyen, T. Nguyen, N. Tuan, N. Cuong, N. Kien, P. Huy, V. Hieu Nguyen, and D. Nguyen, *J. Lumin.*, 2014, **156**, p 199.
48. P. Shankar, and J. Bosco Balaguru Rayappan, P. Shankar, and J. Bosco Balaguru Rayappan, *J. Mater. Chem. C*, 2017, **5**, p 10869.
49. Y. Yoon, K. Park, and S. Kim, Y. Yoon, K. Park, and S. Kim, *Thin Solid Films*, 2015, **597**, p 125.
50. K. Gautam, I. Singh, P. Bhatnagar, and K. Rao Peta, K. Gautam, I. Singh, P. Bhatnagar, and K. Rao Peta, *Superlattices Microstruct.*, 2016, **93**, p 101.
51. N. Basinova, O. Cernohorsky, J. Grym, S. Kucerova, H. Faitova, R. Yatskiv, J. Vanis, J. Vesely, and J. Maixner, N. Basinova, O. Cernohorsky, J. Grym, S. Kucerova, H. Faitova, R. Yatskiv, J. Vanis, J. Vesely, and J. Maixner, *Crystals*, 2019, **9**, p 566.
52. M. Desai, V. Sharma, M. Prasad, S. Jadhkar, G. Saratale, and S. Sartale, M. Desai, V. Sharma, M. Prasad, S. Jadhkar, G. Saratale, and S. Sartale, *Int. J. Hydrog. Energy*, 2020, **45**, p 5783.

53. N. Syafinaz Ridhuan, K. Abdul Razak, Z. Lockman, and A. Abdul Aziz, N. Syafinaz Ridhuan, K. Abdul Razak, Z. Lockman, and A. Abdul Aziz, *PLoS ONE*, 2012, **7**, p e50405.
54. A. Abdulrahman, S. Ahmed, N. Ahmed, and M. Almessiere, A. Abdulrahman, S. Ahmed, N. Ahmed, and M. Almessiere, *Dig. J. Nanomater. Biostruct.*, 2016, **11**, p 1007.
55. S. Ahmed, S. Ahmed, *Rev. Innovaciencia*, 2018, **6**, p 1.
56. U. Holzwarth, and N. Gibson, U. Holzwarth, and N. Gibson, *Nat. Nanotechnol.*, 2011, **6**, p 534.
57. A. Faisal, R. Ismail, W. Khalef, and E. Salim, A. Faisal, R. Ismail, W. Khalef, and E. Salim, *Opt. Quantum Electron.*, 2020, **52**, p 1.
58. A. Abdulrahman, S. Ahmed, N. Ahmed and M. Almessiere, in *AIP Conference Proceedings* (AIP Publishing LLC, 2017), p. 20004.
59. P. Sundara Venkatesh, V. Purushothaman, S. Esakki Muthu, S. Arumugam, V. Ramakrishnan, K. Jeganathan, and K. Ramamurthi, P. Sundara Venkatesh, V. Purushothaman, S. Esakki Muthu, S. Arumugam, V. Ramakrishnan, K. Jeganathan, and K. Ramamurthi, *Cryst. Eng. Commun.*, 2012, **14**, p 4713.
60. K. Onlaor, N. Chaithanatkun, and B. Tunhoo, K. Onlaor, N. Chaithanatkun, and B. Tunhoo, *Curr. Appl. Phys.*, 2016, **16**, p 1418.
61. M. Gusatti, C. Campos, D. Souza, V. Moser, N. Kuhnen, and H. Riella, M. Gusatti, C. Campos, D. Souza, V. Moser, N. Kuhnen, and H. Riella, *J. Nanosci. Nanotechnol.*, 2013, **13**, p 8307.
62. A. Singh, and H. Vishwakarma, A. Singh, and H. Vishwakarma, *Mater. Sci. Pol.*, 2015, **33**, p 751.
63. R. Yatskiv, and J. Grym, R. Yatskiv, and J. Grym, *Superlattices Microstruct.*, 2016, **99**, p 214.
64. E. Karaköse, and H. Çolak, E. Karaköse, and H. Çolak, *Energy*, 2017, **140**, p 92.
65. S. Lin, H. Hu, W. Zheng, Y. Qu, and F. Lai, S. Lin, H. Hu, W. Zheng, Y. Qu, and F. Lai, *Nanoscale Res. Lett.*, 2013, **8**, p 158.
66. T. Flemban, V. Singaravelu, A. Aravindh Sasikala Devi, and I. Roqan, T. Flemban, V. Singaravelu, A. Aravindh Sasikala Devi, and I. Roqan, *RSC Adv.*, 2015, **5**, p 94670.
67. A. Katoch, G. Sun, S. Choi, J. Byun, and S. Sub Kim, A. Katoch, G. Sun, S. Choi, J. Byun, and S. Sub Kim, *Sens. Actuators B Chem.*, 2013, **185**, p 411.
68. H. Ghayour, H. Rezaie, S. Mirdamadi, and A. Nourbakhsh, H. Ghayour, H. Rezaie, S. Mirdamadi, and A. Nourbakhsh, *Vacuum*, 2011, **86**, p 101.
69. M. Wang, C. Ye, Y. Zhang, G. Hua, H. Wang, M. Kong, and L. Zhang, M. Wang, C. Ye, Y. Zhang, G. Hua, H. Wang, M. Kong, and L. Zhang, *J. Cryst. Growth*, 2006, **291**, p 334.
70. L. Roza, M. Yusri Abd Rahman, A. Umar, and M. Mat Salleh, L. Roza, M. Yusri Abd Rahman, A. Umar, and M. Mat Salleh, *J. Alloys Compd.*, 2015, **618**, p 153.
71. G. Nisha Narayanan, R. Sankar Ganesh, and A. Karthikeyan, G. Nisha Narayanan, R. Sankar Ganesh, and A. Karthikeyan, *Thin Solid Films*, 2016, **598**, p 39.

**Publisher's Note** Springer Nature remains neutral with regard to jurisdictional claims in published maps and institutional affiliations.